Journal of Crystal Growth 312 (2010) 656–661

Contents lists available at ScienceDirect

Journal of Crystal Growth

journal homepage: www.elsevier.com/locate/jcrysgro

High yield–low temperature growth of indium sulphide nanowires via chemical vapor deposition

Matthew Zervos [a,*], Pola Papageorgiou [b], Andreas Othonos [b]

[a] Nanostructured Materials and Devices Laboratory, Department of Mechanical Engineering, Materials Science Group, University of Cyprus, Kalipoleos 75, 1678, Nicosia P.O. Box 20573, Cyprus

[b] Research Centre of Ultrafast Science, Department of Physics, University of Cyprus, Kalipoleos 75, 1678, Nicosia P.O. Box 20573, Cyprus

ARTICLE INFO

Article history:
Received 2 September 2009
Received in revised form
19 November 2009
Accepted 8 December 2009
Communicated by J.M. Redwing
Available online 16 December 2009

Keywords:
A1. Nanostructures
A3. Chemical vapor deposition processes
B1. Nanomaterials
B1. Sulfides
B2. Semiconducting materials

ABSTRACT

Indium sulphide nanowires (NWs) have been grown on Si via the reaction of In and $InCl_3$ with H_2S using chemical vapor deposition at temperatures as low as 250 °C. We find that the growth of In_xS_y NWs via the direct reaction of In with H_2S is hindered by the formation of In_xS_y around the source of In which limits its vapor pressure. Thus a low yield of In_xS_y NWs with diameters of ≈ 100 nm, lengths up to ≈ 5 μm and hexagonal crystals measuring ≈ 500 nm across, were obtained between 500 and 600 °C, but their growth was not uniform or reproducible. These exhibited weak, but nevertheless clear peaks, in the X-ray diffraction (XRD) spectrum corresponding to tetragonal β-In_2S_3 and orthorhombic InS. No NWs were obtained for $T_G \leq 500$ °C while for $T_G > 600$ °C we obtained a polycrystalline layer with oriented grains of triangular shape. In contrast, a high yield of InS NWs with diameters ≤ 200 nm and lengths up to ≈ 2 μm were obtained at temperatures as low as 250 °C via the reaction of In and $InCl_3$ with H_2S. The sublimation of $InCl_3$ enhances the vapor pressure of In and the growth of InS NWs, which organize themselves in urchin like structures at 300 °C, exhibiting very intense peaks in the XRD spectrum, corresponding mainly to orthorhombic InS. Optical transmission measurements through the InS NWs gave a band-gap of 2.4 eV.

1. Introduction

Indium sulphide has been receiving increasing attention over the past years due to its application in second generation, thin film solar cells as an alternative to CdS and its intermediate band-gap of 2.0–2.8 eV [1,2]. Indium sulphide (In_xS_y) is a III–VI semiconductor and may exist in the cubic α-In_2S_3, tetragonal β-In_2S_3 trigonal γ-In_2S_3 or orthorhombic InS form [3]. Thin films (TFs) of In_xS_y have been grown so far by a variety of methods including metal-organic chemical vapor deposition (MOCVD) [1], spray [4–6], chemical bath [7,8], thermal evaporation [9–11] and spin coating [12] methods. Most of the In_xS_y TFs are actually polycrystalline and each has specific crystal, electrical and optical properties depending on the method of deposition used. Despite the fact that their properties show variation and depend strongly on the growth method, high efficiency solar cells have been fabricated from such TFs [13] and many of these are structured on the nanometer scale [14]. In contrast to TFs, nanostructured In_xS_y such as nanorods (NRs) [14] nanoparticles (NPs) [15], nanocrystals (NCs) [11,16,17], nanowires (NWs) [18,19] and larger structures such as dandelion flowers (FWs) [20] and urchin-like spheres [21] have been grown mainly by hydro or solvo-thermal [18,20,21,28] and sol–gel [16,17] methods which however take too long, involve complicated chemical reactions and as a consequence cannot be easily optimized. Specifically, In_2S_3 NWs with diameters of 10 nm have been grown over 15 h in porous alumina membranes (PAMs) using the hydrothermal method by Zhu et al. [19] while Datta et al. obtained InS and β-In_2S_3 NWs with diameters between 40 and 140 nm using the solvo-thermal method [18] over 16 h as the temperature was changed between 190 and 280 °C. More recently In_2S_3 zig–zag NWs with average diameter of 66 nm and lengths 1–2 μm were grown by Datta et al. [27] in a different way i.e. via a high temperature thermal evaporation route and the reaction of In with S in solid form. These In_2S_3 zig–zag NWs exhibited high luminescence and rectifying behavior.

Consequently there are only few investigations into the growth of In_xS_y NWs despite the fact that a great variety of semiconductor NWs have been grown over the past few years and used for the fabrication of nanoscale devices. Therefore we have carried out a detailed, systematic, study into the growth of In_xS_y nanostructures via the reaction of In and/or $InCl_3$ with H_2S using atmospheric pressure chemical vapor deposition over a broad temperature range i.e. T_G=200–800 °C which is not so time

* Corresponding author. Tel.: +357 22892194; fax: +357 22892254.
E-mail address: zervos@ucy.ac.cy (M. Zervos).

0022-0248/$ - see front matter © 2009 Elsevier B.V. All rights reserved.
doi:10.1016/j.jcrysgro.2009.12.023

consuming as hydro or solvo-thermal methods. We find that the growth of In_xS_y NWs via the direct reaction of In with H_2S is difficult and complicated by the formation of an In_xS_y shell around the molten source of In which limits its vapor pressure significantly. Only a low yield of In_xS_y NWs with diameters of ≈ 100 nm and lengths up to ≈ 5 μm or hexagonal crystals were obtained in the temperature range 500–600 °C corresponding to tetragonal β-In_2S_3 and orthorhombic InS, but not in a reproducible fashion. No nanostructures were obtained for $T_G \leq 500$ °C due to the extremely low vapor pressure of In while for $T_G > 600$ °C we obtained a polycrystalline layer of In_xS_y with oriented grains of triangular shape.

The difficulties associated with the yield and reproducibility were overcome by using $InCl_3$ which undergoes sublimation i.e. $InCl_3(s) \rightarrow InCl_3(g)$ and therefore acts as a dispersant and a shield against the reactive H_2S. This in turn enhances the vapor pressure of In and as a consequence the one dimensional (1D) growth of InS NWs at temperatures as low as 250 °C. Increasing the reaction temperature leads to the formation of more complex structures such as urchin-like structures and flat hexagonal crystals corresponding mainly to tetragonal β-In_2S_3 but also with an orthorhombic InS phase whose presence disappears completely at 600 °C. The low temperature, reproducible growth of InS NWs with a high yield demonstrated on quartz, is important for the fabrication of third generation solar cells on cheap substrates such as glass.

2. Experimental

The In_xS_y nanostructures were grown using an atmospheric pressure chemical vapor deposition (APCVD) system that consists of four mass flow controllers (MFC's) and a horizontal tube furnace, capable of reaching a maximum temperature of 1100 °C. More specifically In_xS_y nanostructures were grown on n^+ Si(1 1 1) covered with a thin layer of Au that had a thickness of a few nanometers. The Au/Si samples had an area ≈ 7 mm $\times$ 7 mm and the Au was deposited using an Ar plasma under a pressure $< 10^{-2}$ mBar. In order to grow In_xS_y nanostructures we used ≈ 0.1 g of fine In powder (Aldrich, Mesh-100, 99.99%) and/or $InCl_3$ (Aldrich 99.999%) that were loaded either separately or together in the centre of a porcelain boat. The Au/Si sample was positioned ≈ 5 mm away from the solid precursor(s) and subsequently the boat was loaded into the 25 mm diameter quartz tube, at its centre and directly above the thermocouple used to measure the heater temperature. Upon loading the boat at room temperature (RT), nitrogen N_2 (99.999%) containing 5% of H_2, i.e. N_2:5% H_2 was introduced at 500 standard cubic centimetres per minute (sccm's) along with 500 sccm's of Ar for 15 min in order to purge the tube and eliminate oxygen and moisture. Following this the temperature was ramped to the desired growth temperature (T_G) using a typical ramp rate of 20 °C/min in a reduced gas flow of 100 sccms N_2:5% H_2. Upon reaching T_G, H_2S was introduced at 15 sccm's for a further 60 min either on its own or along with 85 sccms of N_2:5% H_2 for the purpose of diluting the H_2S after which the tube was allowed to cool down using the same flow of gasses employed during the growth step over a period of 45 min. The reactor was finally purged with 500 sccms of N_2:5% H_2 and 500 sccms of Ar in order to eliminate the H_2S and the boat was removed from the tube only when the temperature was < 100 °C. The morphology of the In_xS_y nanostructures were examined with a TESCAN scanning electron microscope (SEM) while their crystal structure and the phase purity were investigated using a SHIMADZU, XRD-6000, X-ray diffractometer with Cu-Ka source by performing a scan of θ–2θ in the range 10–80°. For optical measurements, In_xS_y nanostructures were grown directly onto square pieces of quartz with an area of ≈ 7 mm $\times$ 7 mm also coated with a few nanometers of Au. Steady state optical spectroscopy was carried out using a Perkin Elmer Lambda 950 standard UV/V spectrophotometer in the transmission mode and normal incidence.

3. Results and discussion

We will begin by considering the growth of In_xS_y NWs via the direct reaction of In with H_2S in order to gain an understanding of the difficulties involved with attaining a high yield, then we shall discuss how these were overcome using $InCl_3$, by describing first of all the reaction of $InCl_3$ alone with H_2S and secondly the optimum reaction of In and $InCl_3$ with H_2S which lead to a high yield of InS NWs at low temperatures.

Indium has a relatively low melting point of 156 °C and reacts readily with H_2S leading to the formation of In_xS_y. The growth of In_xS_y NWs on Si is complicated by the growth of In_xS_y on the surface of the molten source of In situated upstream from the Si, which reduces significantly its vapor pressure. To be specific the In_xS_y that grows on the surface of the molten In during its reaction with H_2S is a shell that consists of 'needle' like structures which grow at near right angles to the surface. Such a vapor-limiting shell also occurs with the growth of metal-oxide NWs, e.g. SnO_2, In_2O_3 NWs [25] or nitrides e.g. GaN or InN NWs [26] whereby an oxide or nitride vapor-limiting shell develops around the molten source of the constituent metal as it reacts with O_2 or NH_3 respectively. It has to be emphasized however that the adverse effect of the vapor-limiting shell that occurs from the reaction of In with H_2S is much worst by comparison and for this reason large gas flows were deliberately avoided in an attempt to maintain a substantial partial vapor-pressure of In over the Si for the growth of In_xS_y NWs. Therefore a typical flow rate of 15 sccm's of H_2S was used only during the growth and cool down periods. Admitting H_2S into the reactor at the beginning of the temperature ramp, merely promoted the growth of the vapor-limiting shell which reduced even further the efficiency by which In is transferred into the gas stream. As stated above no nanostructured materials were obtained from the direct reaction of In with H_2S for $T_G < 500$ °C. However, for $T_G = 500$ °C we obtained a low yield of straight In_xS_y NWs with diameters of ≈ 100 nm and lengths up to ≈ 5 μm while hexagonally shaped In_xS_y NCs were obtained at $T_G = 600$ °C. The growth was not at all reproducible or uniform and moreover while tetragonal β-In_2S_3 XRD peaks were always detected for $2\theta < 40°$ those belonging to orthorhombic InS for $2\theta > 40°$ were not. Different growth strategies were employed to circumvent the adverse effect of the vapor-limiting shell and obtain reproducible growth e.g. by admitting H_2S into the reactor at the beginning of the growth step for short intervals e.g. 30, 60 and 180 s and by changing the gas flow of H_2S between 10 and 30 sccm's but we did not observe any systematic trend in the growth of the nanostructures due to these changes within the temperature range $T_G = 500$–600 °C. For $T_G > 600$ °C however we find that there is significant deposition on the Si due to the larger vapor pressure of In which most likely counteracts the action of the vapor-limiting shell. In particular for $T_G = 800$ °C we observed the formation of a polycrystalline thin film (TF) with oriented grains of triangular shape, extending over hundreds of microns. Interestingly branched In_xS_y NWs on top of the polycrystalline TF were also obtained in the high temperature regime with lengths of a few tens of microns but again their distribution was not uniform and their yield limited.

In an attempt to obtain a high yield of In_xS_y NWs we also tried carrying out a direct reaction of In thin layers with H_2S. The thin layers of In that were prepared had thicknesses of 10, 20, 30, 40, 100 and 300 nm and were deposited by thermal evaporation

using high purity 99.99% In wire on ≈ 1.0 nm Au/Si(0 0 1). Subsequently the In TFs were allowed to react with 15 sccm's of H_2S in the APCVD reactor described above, at T_G=500 °C. While In_xS_y NWs were obtained in this way, they were dispersed among large, irregular droplets of In especially in the case of the thick In layers. Interestingly, closed packed NPs with average diameters of ≈ 200 nm were obtained in the case of thin In layers which extended over several hundreds of microns, displaying planar dendrite geometries similar to hierarchical self assembly of NPs achieved by Datta et al. via precipitation [22]. Although In_xS_y NWs were observed after the exposure of the thin layers of In to the H_2S they did not exceed 1 μm lengths and were not straight but bent and 'fat'. In short the direct reaction of In with H_2S does not lead to reproducible, uniform and high yield growth of In_xS_y NWs.

The poor yield, bad uniformity and also lack of reproducibility associated with the synthesis of In_xS_y NWs via the direct reaction of In with H_2S were alleviated by adding $InCl_3$ which undergoes total sublimation at 500 °C i.e. $InCl_3(s) \rightarrow InCl_3(g)$, thereby providing substantial vapor to the gas stream and preventing the formation of a vapor-limiting shell around the In. However before considering in detail the growth of In_xS_y nanostructures obtained from the reaction of In and $InCl_3$ with H_2S it is instructive to describe the reaction of $InCl_3$ alone with H_2S. Here we ought to point out that $InCl_3$ has been used in solution for the synthesis of In_2S_3 via the spray pyrolysis method, whereby the $InCl_3$ is deposited in TF form followed by its conversion to In_2S_3 through exposure to H_2S [4].

As already stated above $InCl_3$ undergoes sublimation and starts releasing a significant amount of vapor above 200 °C [23]. The sublimation of $InCl_3(s)$ and the generation of white $InCl_3(g)$ vapor was clearly observed during the temperature ramp near the cool end of the reactor due to its downstream transfer by the 100 sccm N_2:5% H_2 carrier gas flow. The $InCl_3(g)$ reacted with H_2S during the growth step leading to the growth of dandelion flowers (FWs) on Si at 400 °C with excellent uniformity and high yield, as shown in Fig. 1(a). These are similar to the dandelion FWs obtained by solvothermal methods [20,24]. The In_xS_y FWs have diameters ranging up to 10 μm. The reaction of $InCl_3(g)$ with H_2S lead predominantly to the growth of NPs and chains of NPs at higher temperatures, as shown in Fig. 1(b) with a lower yield compared to that of the dandelion FWs. This is a direct consequence of the longer ramp time and the fact that $InCl_3$ totally dissociates above 500 °C which simply resulted into the transfer of almost all of the $InCl_3$ vapor, downstream towards the cool end of the reactor before any was left to react with the H_2S since the latter was always admitted into the reactor at the beginning of the growth step. However the prolonged duration of the temperature ramp all the way up to 800 °C led to the complete elimination of $InCl_3$ from the boat and its total transfer downstream prior to any reaction with H_2S so no deposition occurred at all on the Si, in contrast to the direct reaction of In with H_2S. The In_xS_y FWs grown at 400 °C exhibited intense peaks in the XRD corresponding to tetragonal β-In_2S for $2\theta < 40^\circ$ peaks and orthorhombic InS for $2\theta > 40^\circ$ as shown in Fig. 1(c). In contrast the XRD peaks corresponding to the NPs of Fig. 1(b) are weaker due to the smaller amount of material.

Although the reaction of In with H_2S and $InCl_3$ with H_2S did not lead to the deposition of any nanostructured materials for $T_G < 400$ °C the combined reaction of In and $InCl_3$ with H_2S lead to the growth of In_xS_y NWs at much lower temperatures, i.e., as low as T_G=250 °C. Mixing $InCl_3$ with In increased significantly the vapor pressure of the In while preventing the formation of a shell around the molten In due to the sublimation of $InCl_3$. In other words, the $InCl_3(g)$ acts as a dispersant and prevents the coagulation of the In but also as a shield against the reactive H_2S which prevents the formation of a vapor-limiting shell around the small In droplets. The higher vapor-pressure in turn lead to a higher yield and uniformity.

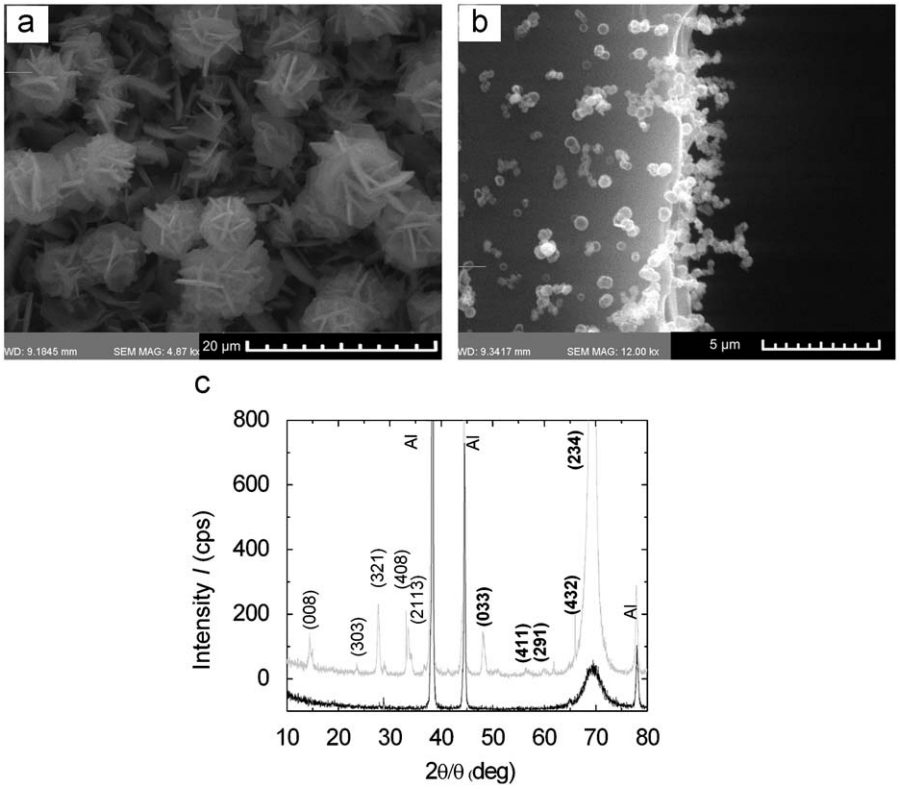

Fig. 1. (a) Dandelion In_xS_y FWs grown at T_G=400 °C from the reaction of $InCl_3$ with 15 sccms of H_2S for 60 min. (b) Nanoparticles obtained at T_G=700 °C with an average diameter of 500 nm. No nanostructures were obtained for $T > 700$ °C, (c) XRD of the dandelion FWs and NPs grown at 400 and 700 °C, top and lower trace respectively.

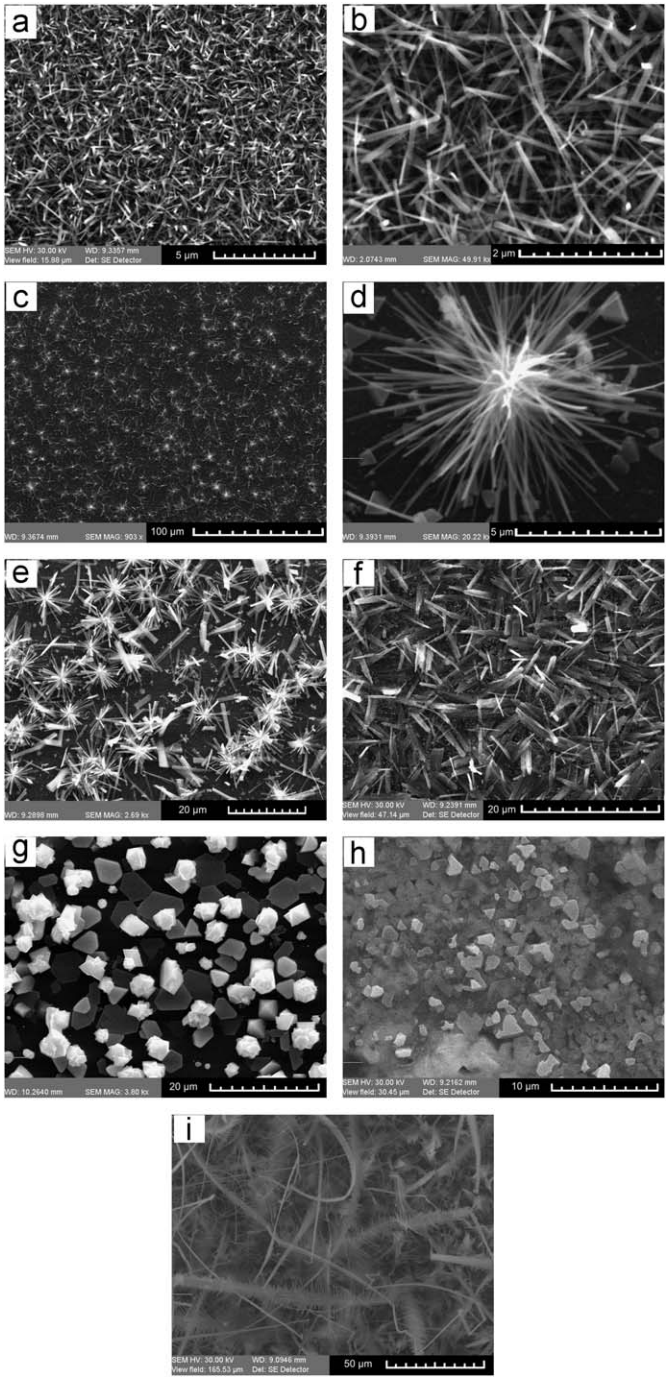

Fig. 2. SEM image of the In_xS_y nanostructures obtained from the reaction of In and $InCl_3$ with 10 sccms H_2S and 90 sccms N_2:5% H_2 (a) InS NWs at T_G=250 °C, (b) T_G=250 °C, close up of InS NWs, (c) T_G=300 °C, InS NWs arranged in urchin like structures which appear as bright spots, (d) T_G=300 °C, close up of urchin structure, (e) T_G=350 °C, needle like In_xS_y mixed with urchin structures, (f) T_G=400 °C, needle like β-In_2S_3, (g) T_G=500 °C, β-In_2S_3 hexagonal NCs, (h), T_G=700 °C β-In_2S_3 polycrystalline TF, (i) T_G=800 °C, branched, feather like NWs.

The In_xS_y nanostructures grown from the reaction of In and $InCl_3$ with H_2S are shown in Fig. 2(a)–(i). A high yield of InS NWs with diameters of $\leq$200 nm and lengths up to $\approx$2 μm were obtained for T_G=250 °C, as can be seen in Fig. 2(a) and (b). However for T_G=300 °C we observe the growth of 500 nm NCs and also $\approx$5 μm long NWs with diameters $<$100 nm which grow in a radial fashion and self assemble into urchin like structures as shown in Fig. 2(c) and (d). Note that the yield and uniformity of In_xS_y NWs in both cases is considerably higher compared to what was obtained in the case of the direct reaction of In with H_2S. The urchin like structures observed for T_G=300 °C persist also when T_G=350 °C as shown in Fig. 2(e) but one can also observe large rods with lengths of 10 μm and diameters $\leq$4 μm. These large structures evolve into longer In_xS_y needle-like crystals at 400 °C as shown in Fig. 2(f). No urchin structures were observed at 400 °C while at 500 °C we obtained a high density of flat hexagonal crystals and small dandelion-like FWs, but no NWs, see Fig. 2(g). The appearance of these well defined hexagonal crystals in fact correspond to the onset in the growth of a polycrystalline TF that clearly occurs at higher temperatures i.e. for T_G=700 °C as can be seen in Fig. 2(h) similar to the case of the direct reaction of In with H_2S. Finally it is interesting to point out that branched and long straight NWs were obtained in the high temperature regime i.e. T_G=700–800 °C as shown in Fig. 2(i) consistent with their presence due to the direct reaction of In with H_2S.

All of the In_xS_y nanostructured materials and also the larger crystals exhibited intense peaks in the XRD spectrum as can be seen in Fig. 3(a) and (b). Considering first the crystal structures obtained for $T_G \geq 400$ °C we find that very intense peaks appear in the XRD spectrum for $2\theta < 40^\circ$ as shown in Fig. 3(b) corresponding to tetragonal β-In_2S_3 which is indicative of their high density and good crystal quality. Note also that these are stronger and more intense than the peaks with $2\theta > 40^\circ$ belonging to the orthorhombic InS phase. This is especially true for the polycrystalline β-In_2S_3 TF where there is a complete suppression of the InS phase and a few of the β-In_2S_3 peaks which is probably indicative of the onset in the formation of γ-In_2S_3 which forms near 800 °C [3]. Here we ought to mention that tetragonal β-In_2S_3 is thermodynamically controlled and requires high temperatures to form [18]. More specifically β-In_2S_3 is known to occur above 330 °C [3] which is consistent with the fact that intense peaks in the XRD with $2\theta < 40^\circ$ corresponding to β-In_2S_3 occurred only for $T_G \geq 400$ °C. These are actually suppressed when $T_G < 400$ °C as can be seen in Fig. 3(a) while at the same time some of the peaks corresponding to orthorhombic InS become comparable in intensity or even larger than those belonging to β-In_2S_3.

It is worthwhile pointing out that the cubic, monoclinic-β and tetragonal crystal structures share a very similar set of peaks for $2\theta < 40^\circ$ but only the tetragonal matches all the observed XRD peaks [18]. On the other hand neither of the cubic, monoclinic-β or tetragonal crystal structures have peaks corresponding to those with $2\theta > 40^\circ$ but only the orthorhombic InS which appears to occur over a broad range of temperatures as can be seen from the XRD spectra of Fig. 3(a) and (b). Consequently we have two phases present in agreement with Datta *et al.* who obtained InS and β-In_2S_3 NWs with diameters between 40 and 140 nm using the solvo-thermal method [18]. For temperatures in the range 190–265 °C they obtained orthorhombic InS while for 275 °C XRD peaks corresponding to tetragonal β-In_2S_3 started making their appearance. However Datta et al. did not grow any In_xS_y NWs at higher temperatures [18] and their XRD spectrum covered only the range 20–60° missing the lowest tetragonal β-In_2S_3 XRD peaks. While the direct reaction of In or $InCl_3$ with H_2S favors the appearance of the orthorhombic InS phase even up to T_G=700 °C we find that the combined reaction of In and $InCl_3$ with H_2S leads to its complete suppression at T_G=600 °C while at the same time nanostructured materials can be grown at much lower temperatures as already discussed in detail above.

In order to obtain a first estimate of the energy bandgap (E_G) of the InS NWs grown via the reaction of In and $InCl_3$ with H_2S at T_G=300 °C we made preliminary measurements of the optical transmission through NWs that were grown directly on quartz with 1.2 nm Au. As can be seen from Fig. 4 we find E_G (InS)=2.4 eV which is consistent with other estimates of the band-gap most of

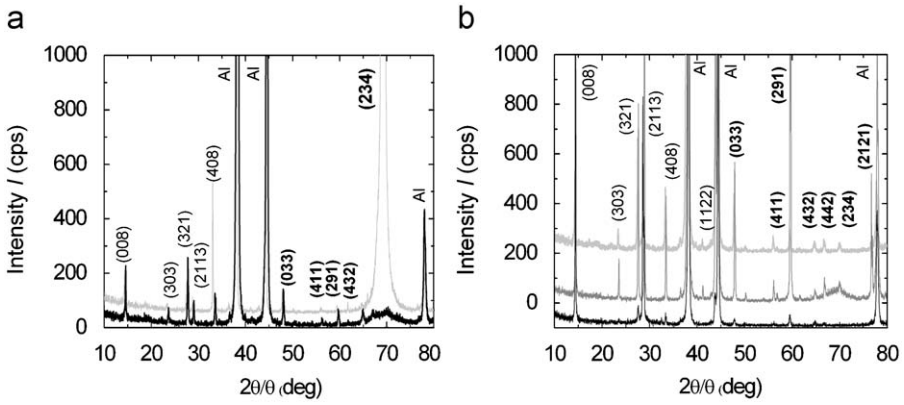

Fig. 3. XRD spectrum of (a) the urchin like structures grown at T_G=300 °C and 350 °C top and bottom line respectively, (b) needle like structures at T_G=400 °C, upper trace; hexagonal crystals grown at T_G=500 °C, middle trace and polycrystalline TF at T_G=600 °C, lower line.

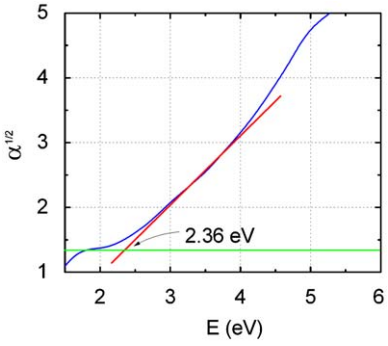

Fig. 4. Square root of the absorption $\alpha^{1/2}$ versus photon energy determined from the transmission spectrum of the InS urchin like structures grown directly on quartz at T_G=300 °C via the reaction of In and $InCl_3$ with H_2S.

which fall in the range 2.0–2.8 eV [2]. A similar band-gap i.e. 2.5 eV was determined for the InS NWs grown directly on quartz at T_G=250 °C. Therefore we find that there are no significant differences between the absorption and transmission spectrum of the InS NWs and those of the InS urchin-like structures grown at low temperatures. Interestingly the photoluminescence (PL) spectrum of the InS NWs is broad and very similar to that obtained by Zhu et al. [19] on indium suplhide nanofibers. It should be noted also that the morphology of the InS NWs and their density on quartz are very similar to those shown in Fig. 2(a)–(c) which were grown on Si. It appears therefore to be possible to grow InS NWs directly on glass at these relatively low growth temperatures which is useful for the fabrication of third generation solar cells. We should finally point out that the size and density of the nanostructures obtained at 250–300 °C is low by comparison to the size and density of the structures obtained for $T_G > 250$ °C. Therefore it was not possible to obtain a clear absorption–transmission spectrum in the latter case. A detailed investigation of the optical properties via steady state and time resolved spectroscopy will be given elsewhere.

4. Conclusions

We have grown orthorhombic InS NWs with diameters of < 100 nm and lengths up to 2 μm with a high yield on Si and quartz via the reaction of In and $InCl_3$ with H_2S at temperatures as low as 250 °C. The InS NWs tend to organize themselves into urchin like structures at 300 °C which evolve into larger, needle like structures corresponding mainly to tetragonal β-In_2S_3 for T_G=400 °C while for temperatures ≥ 500 °C growth proceeds in a two dimensional fashion giving rise to well defined tetragonal β-In_2S_3 flat hexagonal crystals at 500 °C and a polycrystalline TF for $T_G > 500$ °C. While the tetragonal β-In_2S_3 appears at T_G=350 °C, the orthorhombic InS phase is suppressed above $T_G > 350$ °C and completely eliminated at T_G=600 °C.

A high yield and uniform distribution of β-In_2S_3 NWs was not obtained from the reaction of In with H_2S due to the formation of an In_xS_y shell around the In melt which significantly limits its vapor pressure, especially at low temperatures i.e. $T_G < 500$ °C. Even though a low yield of NWs with diameters of 100 nm and lengths of ≈ 5 μm were obtained at 500 °C their growth was not reproducible or uniform. This was overcome via the incorporation of $InCl_3$ which sublimates thereby acting as a dispersant and a shield for the molten In against the reactive H_2S, which as a consequence, enhanced significantly the vapor pressure of In in the main gas stream and the formation of InS NWs at lower temperatures. The high yield of InS NWs obtained via the combined reaction of In and $InCl_3$ with H_2S at low temperatures on quartz is important for the fabrication of third generation solar cells on cheap substrates such as glass.

Acknowledgments

The work in this article was supported by the Research Promotion Foundation of Cyprus (www.research.org.cy) under Grant BE0308/03 for fundamental research in the area of nanotechnology and nanostructured materials.

References

[1] A.N. MacIness, W.M. Cleaver, R. Barron, M.B. Power, A.F. Hepp, Adv. Mater. Opt. Electron. 1 (1992) 229.
[2] N. Barreau, Solar Energy 83 (2009) 363.
[3] W. Rehwald, G. Harbeke, J. Phys. Chem. Solids 26 (1965) 1309.
[4] N.A. Allsop, A. Schönmann, A. Belaidi, H.-J. Muffler, B. Mertesacker, W. Bohne, E. Strub, J. Röhrich, M.C. Lux-Steiner, Ch.-H. Fischer, Thin Solid Films 513 (2006) 52.
[5] M. Mathew, R. Jayakrishnan, P.M.R. Kumar, C.S. Kartha, K.P. Vijayakumar, J. Appl. Phys. 100 (2006) 033504.
[6] K.C. Wilson, T. Sebastia, T.T. John, C.S. Kartha, K.P. Vijayakumar, P. Magudapathi, K.G.M. Nair, Appl. Phys. Lett. 89 (2006) 013510.
[7] C. Lokhande, A. Ennaoui, P.S. Patil, M. Giersig, K. Diesner, M. Muller, H. Tributsch, Thin Solid Films 340 (1999) 18.
[8] B. Asenjo, C. Sanz, C. Guillén, A.M. Chapparro, M.T. Gutiérrez, J. Herrero, Thin Solid Films 515 (2007) 6041.
[9] N. Barreau, S. Marsillac, J.C. Bernede, T. Ben Nasrallah, S. Belgacem, Phys. Status Solidi A 184 (2001) 179.
[10] A.A. El Shazly, D.Abd. Elhay, H.S. Metwally, M.A.M. Seyam, J. Condens. Mater. 10 (1998) 5943.

[11] C. Kaito, A. Ito, S. Kimura, Y. Kimura, Y. Saito, T. Nakada, J. Cryst. Growth 218 (2000) 259.
[12] Y. Yasaki, N. Sonoyama, T. Sakata, J. Electroanal. Chem. 469 (1999) 116.
[13] K. Hara, K. Sayama, H. Arakawa, Sol. Energy Mater. 62 (2000) 441.
[14] A. Datta, S.K. Panda, S. Gorai, D. Ganguli, S. Chaudhuri, Mater. Res. Bull. 43 (2008) 983.
[15] D.P. Dutta, G. Sharma, A.K. Tyagi, S.K. Kulshreshtha, Mater. Sci. Eng. B 138 (2007) 60.
[16] W. Han, L. Yi, N. Zhao, A. Tang, M. Gao, Z. Tang, J. Am. Chem. 130 (2008) 13152.
[17] A. Datta, S. Gorai, S. Chaudhuri, J. Nanopart. Res. 8 (2006) 919.
[18] A. Datta, S. Gorai, S.K. Panda, S. Chaudhuri, Cryst. Growth Des. 6 (2006) 1010.
[19] X. Zhu, J. Ma, Y. Wang, J. Tao, J. Zhou, Z. Zhao, L. Xie, H. Tian, Mater. Res. Bull. 41 (2006) 1584.
[20] S.D. Naik, T.C. Jagadale, S.K. Apte, R.S. Sonawane, M.V. Kulkarni, S. IPatil, S.B. Ogale, B.B. Kale, Chem. Phys. Lett. 452 (2008) 301.
[21] X. Chen, Z. Zhang, X. Zhang, J. Liu, Y. Qian, Chem. Phys. Lett 407 (2005) 482.
[22] A. Datta, S. Gorai, D. Ganguli, S. Chaudhuri, Mater. Chem. Phys. 102 (2007) 195.
[23] B. Brunetti, V. Piacente, P. Scardala, J. Chem. Eng. Data 43 (1998) 101.
[24] X. Cao, L. Gu, L. Zhuge, W. Qian, C. Zhao, Z. Lan, W. Sheng, D. Yao, Colloids Surf. A 297 (2007) 183.
[25] M. Zervos, D. Tsokou, M. Pervolaraki, A. Othonos, Nanoscale Res. Lett. 4 (2009) 491.
[26] M. Zervos, A. Othonos, Nanoscale Res. Lett. 4 (2009) 1103.
[27] A. Datta, G. Sinha, S.K. Panda, A. Patra, Cryst. Growth Des. 9 (2009) 427.
[28] A. Datta, A. Patra, J. Phys. D: Appl. Phys. 42 (2009) 145116.